IN-02-CR
80757

P.34

Semiannual Progress Report No. 5

To

Aircraft Guidance and Controls Branch/489
Guidance and Control Division
National Aeronautics and Space Administration
Langley Research Center
Hampton, VA 23665-5225

For the Grant

PARAMETER IDENTIFICATION FOR NONLINEAR AERODYNAMIC SYSTEMS

Grant No. NAG-1-1065

Period Covered: October 23, 1991 to April 23, 1992

From

Allan E. Pearson
Division of Engineering
Brown University
Providence, Rhode Island 02912

Report Prepared By:

Principal Investigator
Allan E. Pearson

Professor of Engineering
Tele: 401-863-2602
Date: May 7, 1992

Division of Engineering
Carl Cometta

Executive Officer
Tele:401-863-2319
Date: May 7, 1992

Table of Contents

List of Figures

1. Introduction

This Progress Report covers the six month period from October 23, 1991 to April 23, 1992. The completed work during this period is contained in a Ph.D. dissertation of J. Q. Pan and two papers. These are summarized below. Work continues on frequency analysis for transfer function identification, and a new study has been initiated into a "weighted" least squares algorithm within the context of the Fourier modulating function approach. Progress in each of these areas is summarized below. In addition, the first phase of applying these techniques to the F-18 flight data is nearing completion, and these results will also be summarized below.

2. List of Scientific Collaborators: October 23, 1991 to April 23, 1992:

J. Q. Pan	Graduate Student Research Assistant
A. A. Pandiscio	Raytheon Graduate Student Fellow
A. E. Pearson*	Professor and Principal Investigator
Y. Shen*	Graduate Student Research Assistant

*Received partial support under NAG-1-1065.

3. Completed and Continuing Research

3.1. Pan's Ph.D. Dissertation

As implied by the title: *System Identification, Model Reduction and Deconvolution Filtering Using Fourier Based Modulating Signals and High Order Statistics*, J. Q. Pan's Ph.D. dissertation [1] covers a fairly wide range of topics. Some of the results in this thesis have already been summarized in previous reports, and we shall only outline the results here. Thus, Chapter 2 entitled "Input Persistent Excitation and Model Structure Estimation" was discussed in Section 3.2 of Semiannual Progress Report No. 2, and the contents were presented in a short paper entitled "On Order Determination for Linear Differential Scalar Systems" for the 1991 CISS, Johns Hopkins Univ., Baltimore, MD, in March 1991. Parts of Chapter 3 entitled "Frequency Analysis Using Short Time Transient Data" have been discussed in Sections 3.4, 3.2 and 3.3 of Semiannual Progress Reports No's. 2, 3 and 4 respectively, [1] and abbreviated contents were presented in the short paper [2] entitled "Frequency Analysis Via the Method of Moment Functionals" for the 1991 IEEE CDC, Brighton, UK, in December 1991. [2] Chapter 4 entitled "Schemes for Model Reduction and Parameter Identification in the Frequency Domain" is an application to model reduction of our formulation for frequency analysis (Chapter 3) using the Fourier modulating function approach. Two

---

[1] Specifically, that part which deals with single input-single output (SISO) systems. We have since dealt with the MIMO case (see Section 3.7 of [1]), and this will be included in a full-length paper to be written in the near future.

[2] Three preprint copies each of the 1991 CISS and 1991 IEEE CDC papers were mailed to P. C. Murphy on September 13, 1991, along with three copies of the paper entitled "Explicit Least Squares System Parameter Identification for Exact Differential Input/Output Models" which is scheduled to appear in the *Proc. of the Eighth ICMCM*, Pergamon Press, May 1992.

sixth order examples are presented using our method, and these are compared with the reduced order models obtained via two other techniques. We plan to prepare a paper on this chapter after completing a paper on the frequency analysis results. Chapter 5 entitled "High Resolution Frequency Estimation in the Presence of Noise Using Complex Sinusoidal Modulating Signals" involves the classic problem of estimating the frequencies of superimposed sinusoids corrupted by white Gaussian noise. This study was briefly mentioned in Section 3.3 of Semiannual Progress Report No. 4 and was presented as a short paper [3] at the recent 1992 CISS, Princeton Univ., Princeton, NJ, in March 1992. The presentation evoked several inquiries of interest apparently because of its newness to the signal processing audience and the favorable simulation results of this method in comparison with the well-known Yule-Walker equation approach. A full length version of this paper has been submitted for publication to the IEEE Trans. on Signal Processing. Chapter 6 entitled "Deconvolution and Parameter Identification for Noncausal Nonminimum Phase ARMA Systems Using Inverse Cumulants" deals with noncausal discrete-time ARMA models driven by non-Gaussian random inputs possessing nonzero third and fourth order cumulants.

3.2. Weighted Least Squares and Comparison With Other Techniques

We have begun to examine various ways to ameliorate the deleterious effects of noise beyond that which is obtained by our deterministic least squares setting of the Fourier based modulating function technique. We have found that a "weighted" least squares approach seems to hold significant promise, at least for linear system models. To describe these results, consider the SISO linear system model:

$$A(p)y(t) = B(p)u(t) + e(t), \quad 0 \le t \le T \tag{1}$$

where $(A(p),B(p))$ are differential operators, i.e., polynomials in $p=d/dt$, of *a priori* order n, and $e(t)$ represents the effect of modeling errors. Thus far we have considered the weighting situation only for the parametric identification problem, i.e., estimating the coefficients in $(A(p),B(p))$ given the i/o data $[u(t),y(t)]$ on $[0,T]$, but we shall eventually investigate extending the approach to the nonparametric problem as well, i.e., estimating the frequency function $H(i\omega)=B(i\omega)/A(i\omega)$ given transient i/o data on several intervals $[t_r,t_r+T]$, $r=1,2 \cdots N$.

To encompass stochastic models, a first question might be: What is the effect of the modulation process on a continuous-time "white noise" process? To answer this, let us refer to the complex form of the Fourier modulating functions of order n which were defined by Eqs. (2) and (3) in Semiannual Progress Report No. 4, i.e.,

$$\phi_m(t) = e^{-im\omega_0 t}(e^{-i\omega_0 t}-1)^n, \quad 0 \le t \le T = 2\pi/\omega_0 \tag{2}$$

and its equivalent representation (which follows from the binomial expansion) given by

$$\phi_m(t) = e^{-im\omega_0 t} \sum_{k=0}^{n} (-1)^{n-k} \binom{n}{k} e^{-ik\omega_0 t}. \tag{3}$$

In the above, $i=\sqrt{-1}$, m is any integer which we shall refer to as the 'modulating frequency index', $\omega_0=2\pi/T$ plays the role of a "resolving" frequency, and n corresponds to the order of the differential operator model under investigation. Defining a column vector $\theta = \mathrm{col}[-a_1, \cdots -a_n, b_1, \cdots b_n]$, and applying the **Modulation Property**, which is embodied in

Eq. (4) of Semiannual Progress Report No. 4, the modulated version of the model (1) can be put into the (complex valued) linear regression equation format:

$$\gamma_0^y(m) = \gamma(m)\theta + \varepsilon(m), \quad m=0,1,2 \cdots \tag{4}$$

where the row vector of regressors $\gamma(m)$ is defined by

$$\gamma(m) = \text{row}[\gamma_1^y(m), \cdots \gamma_n^y(m), \gamma_1^u(m), \cdots \gamma_n^u(m)] \tag{5}$$

and the $(\gamma_j^u(m), \gamma_j^y(m))$ are defined by [3]

$$\gamma_j^u(m) = \Delta^n (im\,\omega_0)^{n-j} U(m), \quad \gamma_j^y(m) = \Delta^n (im\,\omega_0)^{n-j} Y(m). \tag{6}$$

The residuals for (4) are given by

$$\varepsilon(m) = \int_0^T e(t)\phi_m(t)dt. \tag{7}$$

If we assume that the modeling error function $e(t)$ in (1) is a zero mean Gaussian stationary white noise process with covariance $Ee(t)e(t+\tau)=\sigma\delta(\tau)$ then the question posed at the start of the previous paragraph has a nice closed-form answer in that the covariance of the residuals $\varepsilon(m)$ defined in (7) is found to be given by

$$E\,\varepsilon(m)\varepsilon(m+l) = \begin{cases} \dfrac{\sigma^2}{T}(-1)^l \dfrac{(2n)!}{(n-l)!(n+l)!}, & -n \le l \le n \\ 0 \text{ for all } l \text{ such that } |\,l\,| > n\,. \end{cases} \tag{8}$$

If the residuals in the time domain were indeed white, then weighting the frequency domain residuals $\varepsilon(m)$ by the inverse of the Toeplitz matrix W deduced from (8), i.e., for all frequencies $m=0,1 \cdots M$,

$$\{W\}_{m,m+l} = \begin{cases} (-1)^l \dfrac{(2n)!}{(n-l)!(n+l)!}, & -n \le l \le n \\ 0 \text{ for all } l \text{ such that } |\,l\,| > n \end{cases} \tag{9}$$

would lead to a Gauss-Markov estimate. Although we cannot achieve the minimum variance of a Gauss-Markov estimate, due to the statistical dependence of the regressors on the noise $e(t)$, weighting by the inverse of W seems reasonable for a first attempt at reducing the variance when the measurement noises are white. Employing this weighting and taking into account both the real and imaginary parts of the regressors, the cost function takes the form

$$J = (Y_c - \Gamma_c\theta)' W_c^{-1} (Y_c - \Gamma_c\theta) \tag{10}$$

where the following notation applies:

$$\Gamma_c' = [\ \text{Re}\ (\gamma(0), \cdots \gamma(M)\ ),\ \text{Im}\ (\gamma(0), \cdots \gamma(M)\ )\ ] \tag{11}$$

$$Y_c' = [\ \text{Re}\ (\gamma_0^y(0), \cdots \gamma_0^y(M)\ ),\ \text{Im}\ (\gamma_0^y(0), \cdots \gamma_0^y(M)\ )\ ] \tag{12}$$

with $(\gamma(m), \gamma_0^y(m)\ )$ defined in (5) and (6), and the composite weighting matrix W_c is defined

---

[3] Refer to Eq. (4), also Fig. 1, of the Semiannual Progress Report No. 4 for further details, including the display of the n^{th} order finite difference operator Δ^n.

by

$$W_c = \begin{bmatrix} W & 0 \\ 0 & W \end{bmatrix}. \tag{13}$$

The one-shot parameter estimate which minimizes (10) is given by

$$\hat{\theta}_{wls} = (\Gamma_c' W_c^{-1} \Gamma_c)^{-1} \Gamma_c' W_c^{-1} Y_c. \tag{14}$$

The ordinary least squares estimate (the one we have been working with up till now) is obtained from (14) by setting $W_c = I$, i.e.,

$$\hat{\theta}_{ls} = \left[\Gamma_c' \Gamma_c\right]^{-1} \Gamma_c' Y_c. \tag{15}$$

Shen has compared these two estimates in Monte Carlo simulations for a second order system with white measurement noises (to be summarized below) and indeed the variance of the parameter estimates is reduced in using (14) in relation to (15).

In addition, we are experimenting with an "adaptive" weighting matrix algorithm, which uses the inverse of W_c as a first guess, in an effort to achieve a 'generalized' least squares estimate, thereby further reducing the variance. In this case, the estimate is obtained iteratively by solving for a vector-symmetric matrix pair $(\hat{\theta}_{awls}, W_{awls})$ in a pair of vector-matrix equations which have the following form:

$$\hat{\theta}_{awls} = (\Gamma_c' W_{awls}^{-1} \Gamma_c)^{-1} \Gamma_c' W_{awls}^{-1} Y_c \tag{16}$$

$$W_{awls} = g(\hat{\theta}_{awls}) \tag{17}$$

where the function $g(\hat{\theta}_{awls})$ is the covariance of the residuals as calculated from the model relative to the current estimate of the parameters, $\hat{\theta}_{awls}$, while assuming white independent measurement noises on both the input and output signals for this calculation. The standard relaxation algorithm for solving this nonlinear pair is to first guess $W_{awls} = W_c$ in (16) in order to obtain a first guess for $\hat{\theta}_{awls}$, substitute this value into the RHS of (17), thus obtaining a new value for W_{awls}, which is reinserted into the RHS of (16) to obtain the next value for $\hat{\theta}_{awls}$, etc. [4] This algorithm works quite well with a suitable stopping rule based upon a chosen threshold for change in the estimate of $\hat{\theta}_{awls}$. Convergence has usually been obtained in five to ten iterations for our applications.

To compare the above least squares formulations, consider the second order system $\ddot{y}(t)+3\dot{y}(t)+8y(t)=5u(t)$, $0 \le t \le T$, which possesses the transfer function

$$H(s) = \frac{5}{s^2 + 3s + 8},$$

with the output $y(t)$ corrupted by additive white Gaussian measurement noise. Two hundred Monte Carlo runs were made for each of several noise-to-signal ratios. The input was

---

[4] In keeping with the property from (9) that W and hence W_c is bandlimited to n nonzero values on either side of the main diagonal, these iterations are carried out with W_{awls} also bandlimited to n nonzero values off the main diagonal, where n is the order of the model under consideration.

$u(t)=\sin t^2/5$ over a $T=10s$ time interval for each run. The initial conditions were randomized for each run, and the $[0,T]$ time interval was discretized into 256 subintervals so that a standard $256=2^8$ point DFT/FFT could be used in calculating the Fourier series coefficients of the i/o data for the least squares problems. [5] The results are shown in Figs. 1, 2 and 3 for the respective estimates, i.e., Fig.(1) for $\hat{\theta}_{ls}$, Fig. 2 for $\hat{\theta}_{wls}$, and Fig. 3 for $\hat{\theta}_{awls}$. Each figure shows the estimates for the three parameters against the ideal values: $\theta_1=8$, $\theta_2=3$ and $\theta_3=5$, as a function of the RMS noise intensity relative to the uncorrupted signal. The mean and standard deviations are shown for each parameter estimate based upon the 200 Monte Carlo runs at each noise intensity. In terms of variance, there is a roughly 3 fold decrease in comparing the variance estimate based on $\hat{\theta}_{ls}$ verses $\hat{\theta}_{awls}$, with the variance for $\hat{\theta}_{wls}$ being somewhat between $\hat{\theta}_{ls}$ and $\hat{\theta}_{awls}$. The bias is also smaller for $\hat{\theta}_{awls}$ than that for either $\hat{\theta}_{wls}$ or $\hat{\theta}_{ls}$, and takes on significant values only at high noise levels. A more dramatic comparison is shown in Fig. 4 where the algorithm used was the popular Prediction Error Method (PEM) from the Identification Toolbox by L. Ljung in MATLAB. The superiority of the modulating function technique (MFT) is unmistakable in comparing Fig. 4 with Figs. 1-3. A major reason for this is that the MFT does not have to estimate unknown initial conditions. Another reason is due to the fact that the MFT is a direct identification technique for continuous-time models, while the PEM first estimates the parameters for a discrete-time model then converts this to a continuous-time model. Even with the initial conditions fixed at zero and giving the PEM the correct initial state for each run, the MFT algorithm still gave better results (figures omitted) though the comparisons are less dramatic in this case. Moreover, the MFT required less computer time for each set of Monte Carlo runs (about a five to ten fold decrease depending on whether the PEM had to estimate the initial conditions or not).

---

[5] The formula used for these calculations is based on Simpson's rule and is given by Eq. (19) below.

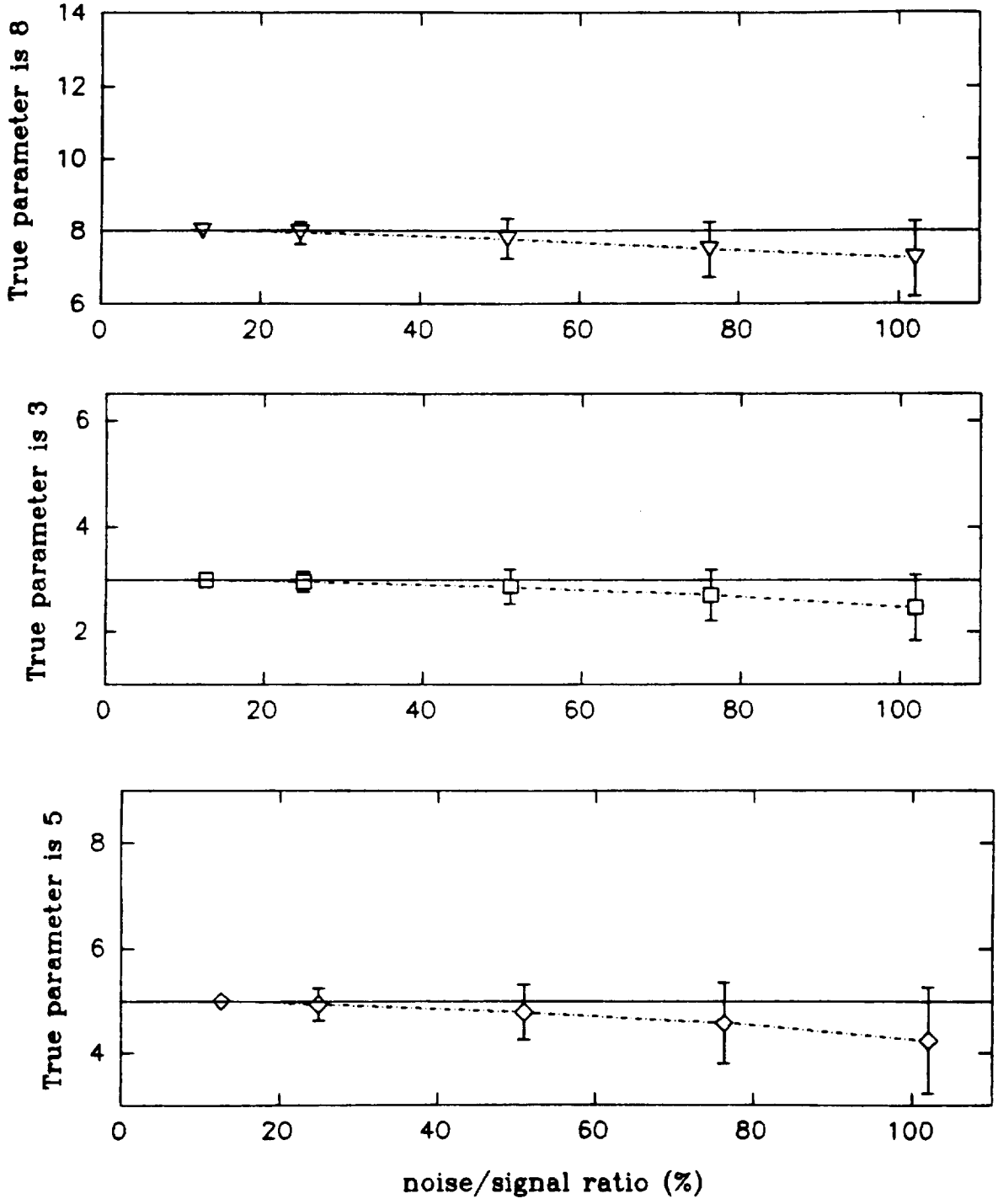

Fig. 1 Performance of the LS Algorithm for Different Noise Levels

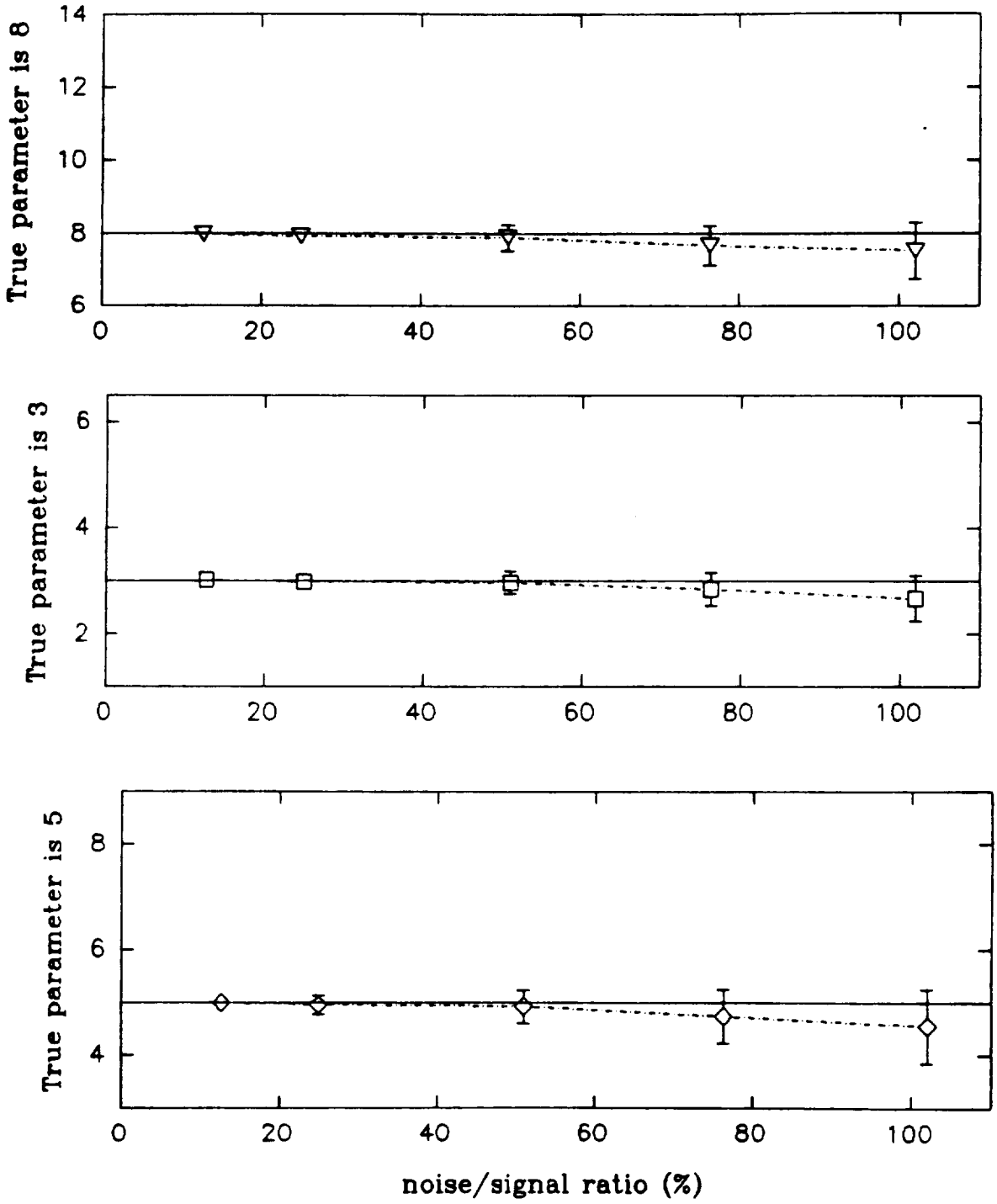

Fig. 2 Performance of the WLS Algorithm for Different Noise Levels

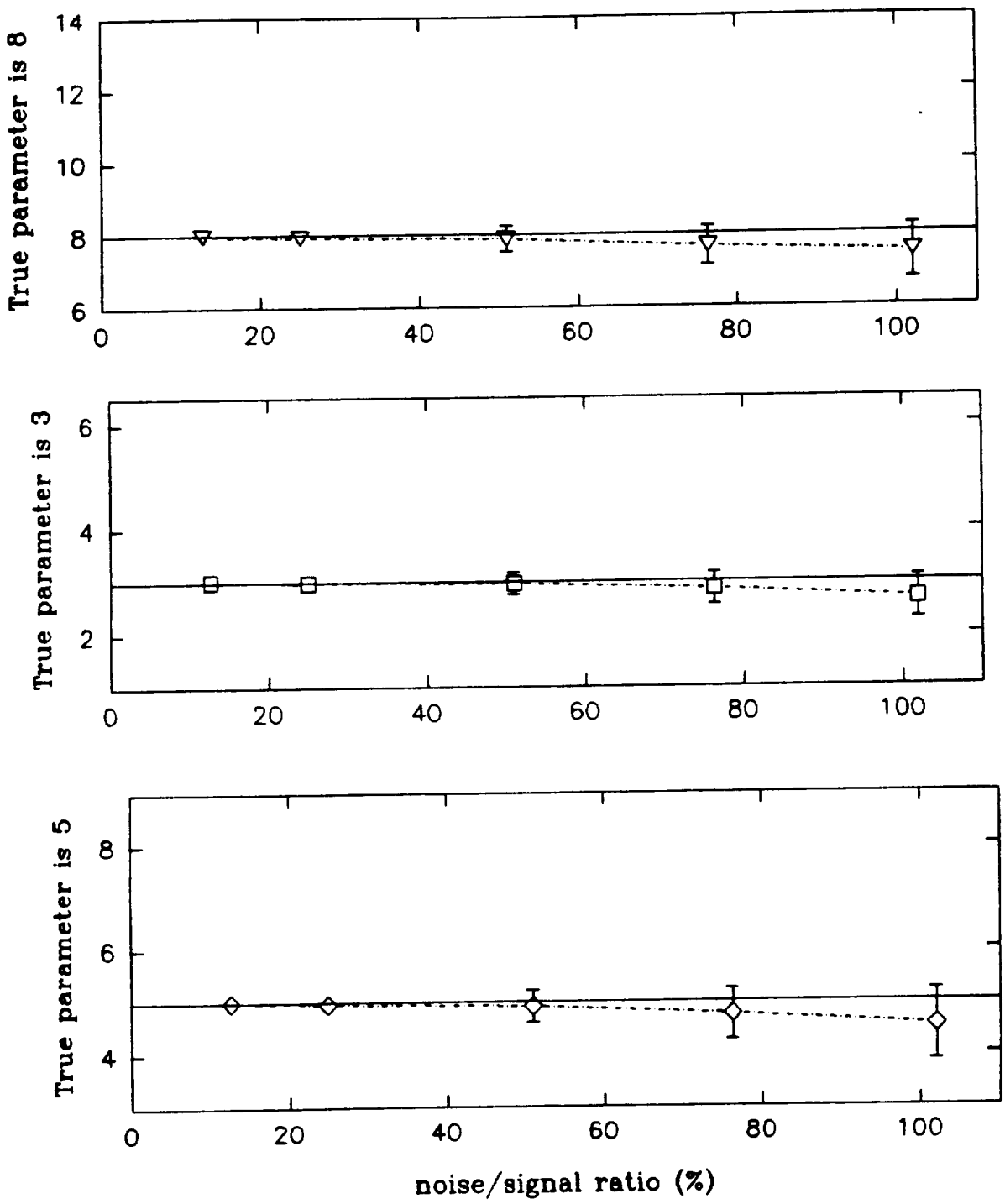

Fig. 3 Performance of the AWLS Algorithm for Different Noise Levels

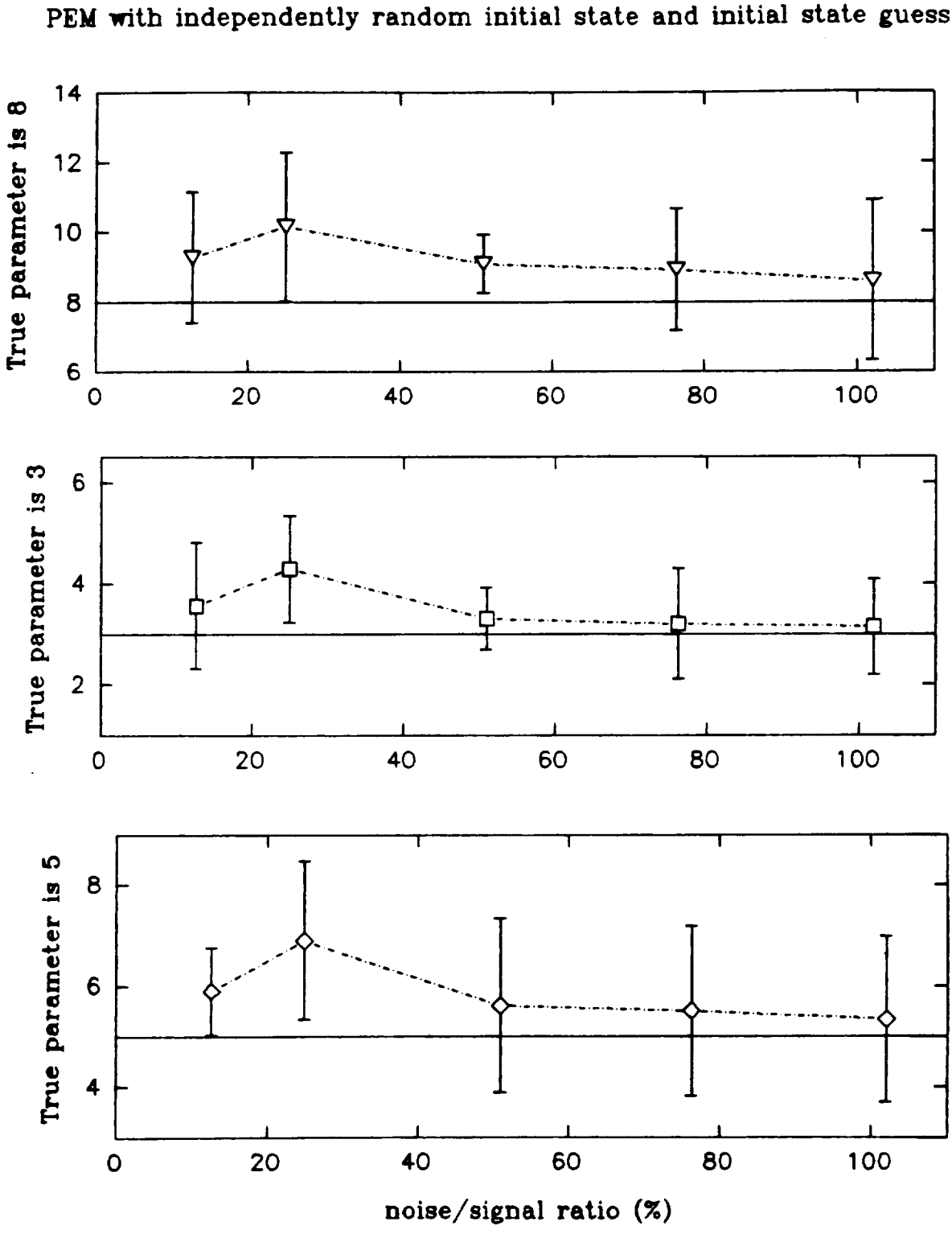

Fig. 4 Performance of the Prediction Error Method for Different Noise Levels

3.3. Modeling the F-18: Phase One Results for Longitudinal Flight

We have begun to model the F-18 aircraft dynamics based upon information communicated to us from Drs. Vlad Klein and Gene Morelli. Yan Shen is assisting in this project. Our initial investigation has focused on the parameter identification problem for the longitudinal dynamics using SISO linear differential operator models of the form represented in (1). In seeking to find the best model within this class, we have to determine the orders of the polynomials $A(p)$ and $B(p)$ as well as their coefficient values. We were given $40.96s$ of data sampled at 50 Hz which means a total of 2250 samples for each signal. Since our algorithms use DFT/FFT techniques to calculate Fourier series coefficients, we truncated the data to 2048 $= 2^{11}$ samples in order to utilize a standard length FFT. The 202 extra data points allowed us to test the sensitivity of the model to shifts in the data sequence. To be specific about the approximations involved, if $z(t)$ is any of the available signals sampled every $\delta t = .02s$ on $[0,T]$ with samples $z_j = z(j\delta t)$, $j = 0,1 \cdots N$, $N = T/\delta t$, then the needed Fourier series coefficients $Z(m)$, $m = 0,1 \cdots M$ were calculated using Simpson's rule, the accuracy of which is of order $(\delta t)^4$:

$$\int_0^T z(t) e^{-im\omega_0 t}\, dt \approx \frac{2\delta t}{3}\left[\frac{z_0+z_N}{2} + \sum_{j=1,3\cdots}^{N-1} 2z_j w_N^{mj} + \sum_{j=2,4\cdots}^{N-2} z_j w_N^{mj}\right], \quad m = 0,1 \cdots M \qquad (18)$$

where $w_N = e^{-i2\pi/N}$. Since N is a power of 2, the above sequence of Fourier series coefficients is represented in row-vector form by the first $M+1$ components of the standard FFT for the sequence inside the brackets on the RHS of (18):

$$Z = \frac{2\delta t}{3}\mathrm{FFT}\left[\frac{z_0+z_N}{2},\ 2z_1,\ z_2,\ 2z_3,\ z_4,\ \cdots 2z_{N-1}\right]. \qquad (19)$$

An inspection of the various signal spectra reveals that the bandwidth of the models will be on the order of 1 Hz or less. Since the resolving frequency is bounded below by the length of the available data, i.e., $f_0 = 1/T = .024414$ Hz or $\omega_0 = 0.15340$ rad/sec, this implies that the number M of modulating functions should be on the order of $M \approx 30$ or 40, else too much noise will be allowed into the least squares regression. This is based on the fact that the highest frequency extracted from the data by the modulating functions is Mf_0Hz, so we impose the constraint: $Mf_0 \approx 1$ Hz. Notice that this implies a usage of only the lower 2% of the available harmonic frequencies in (19) since $N = 2048$. [6]

The longitudinal motion control diagram is shown in Fig. 5 along with the transfer functions of our best models based on the available signals. The Bode plots and impulse responses of the best models are shown in Figs. 6 and 7 for each of the transfer functions. The time domain performance of using these models to predict the outputs in comparison with the physical signals is shown in Fig. 8.

---

[6] The implementation of the n^{th} order finite difference operator Δ^n, which is needed in calculating the regressors (6), actually requires the first $M+n$ harmonics of the Fourier series coefficients of the data. Thus, it is the first $M+n$ components of the FFT sequence (19) which is actually retained in implementing the algorithm, where n is the order of the model under consideration.

F-18 Longitudinal Motion Control Diagram

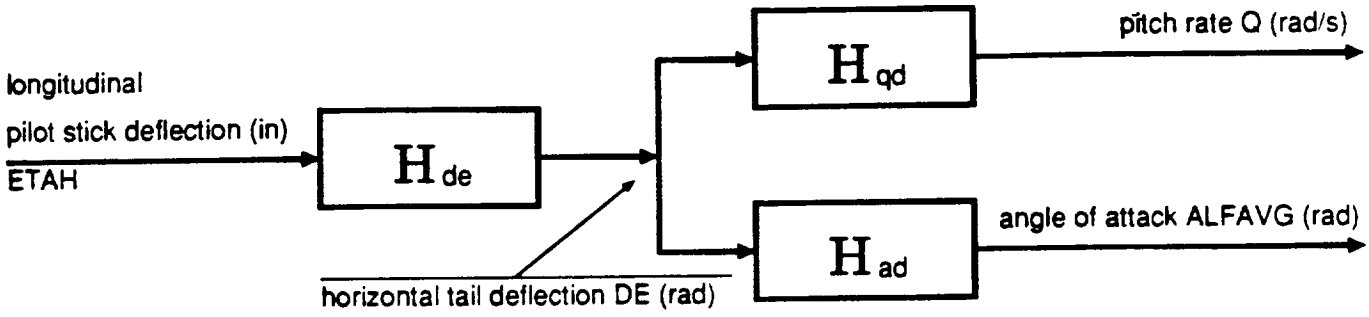

models:

$$H_{de}(s) = \frac{-0.0489s^2 - 0.0244s - 0.0239}{s^2 + 0.1335s + 1.2097}$$

zeros: -0.2497+/-0.6533i

poles: -0.0668+/-1.0978i

$$H_{qd}(s) = \frac{-1.3195s + 0.2457}{s^2 + 0.2465s + 0.0458}$$

zeros: 0.1862

poles: -0.1232+/-0.1750i

$$H_{ad}(s) = \frac{-1.1515}{s^2 + 0.5834s + 0.1064}$$

zeros: none

poles: -0.2916+/-0.1461i

Fig. 5 Block Diagram and the Best Estimated Linear Models

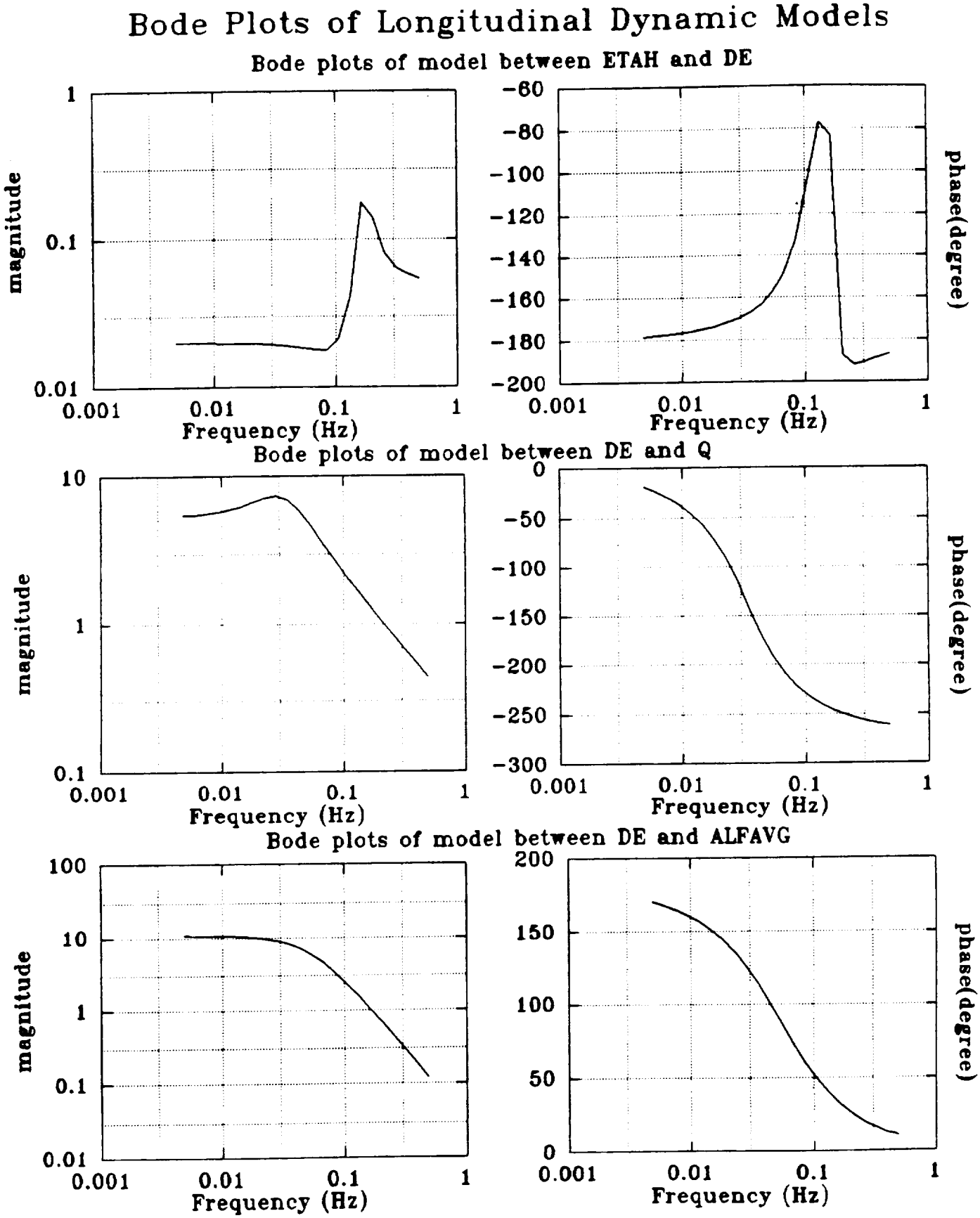

Fig. 6 Bode Plots for $H_{de}(j\omega)$, $H_{qd}(j\omega)$ and $H_{ad}(j\omega)$

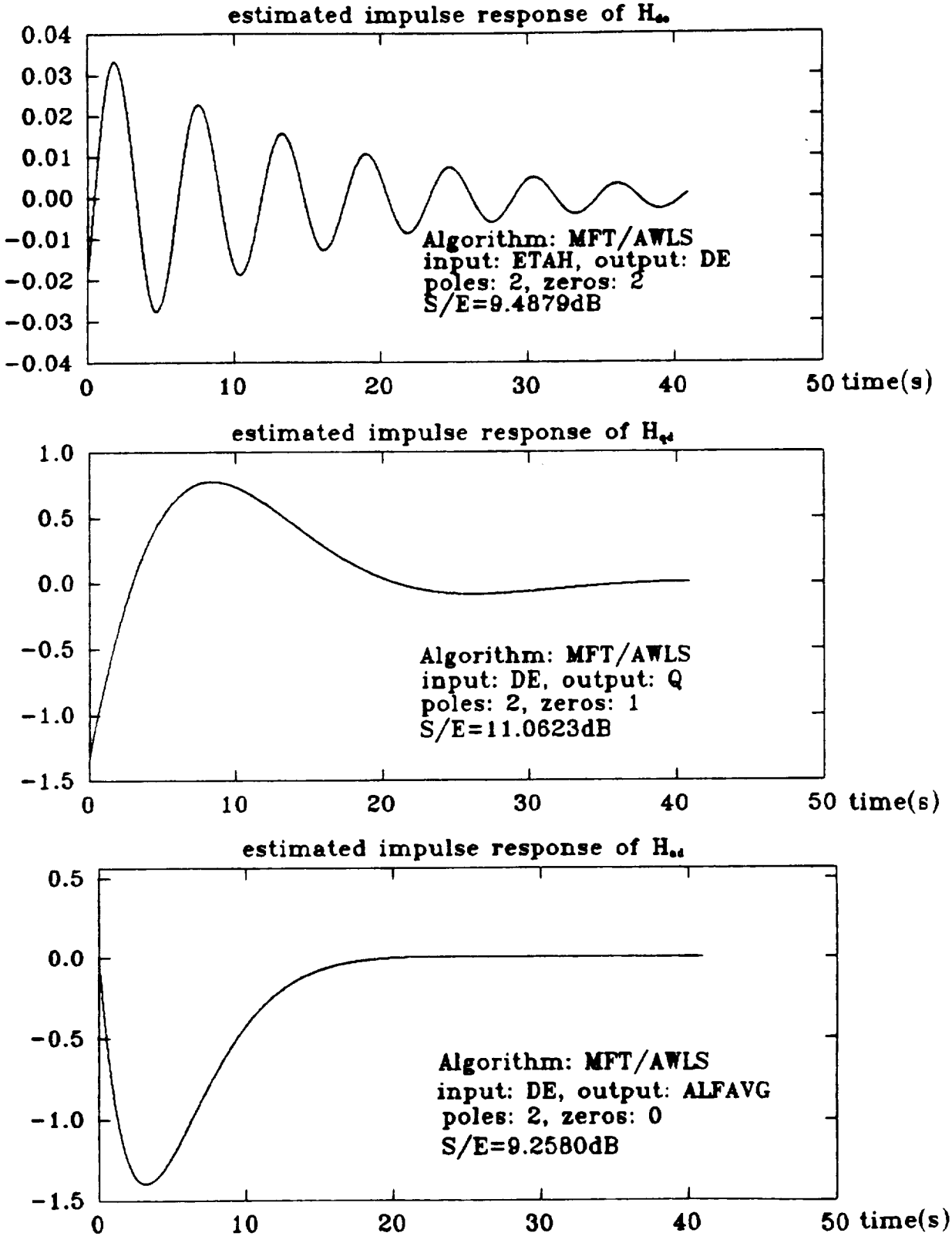

Fig. 7 Impulse Responses for $H_{de}(s)$, $H_{qd}(s)$ and $H_{ad}(s)$

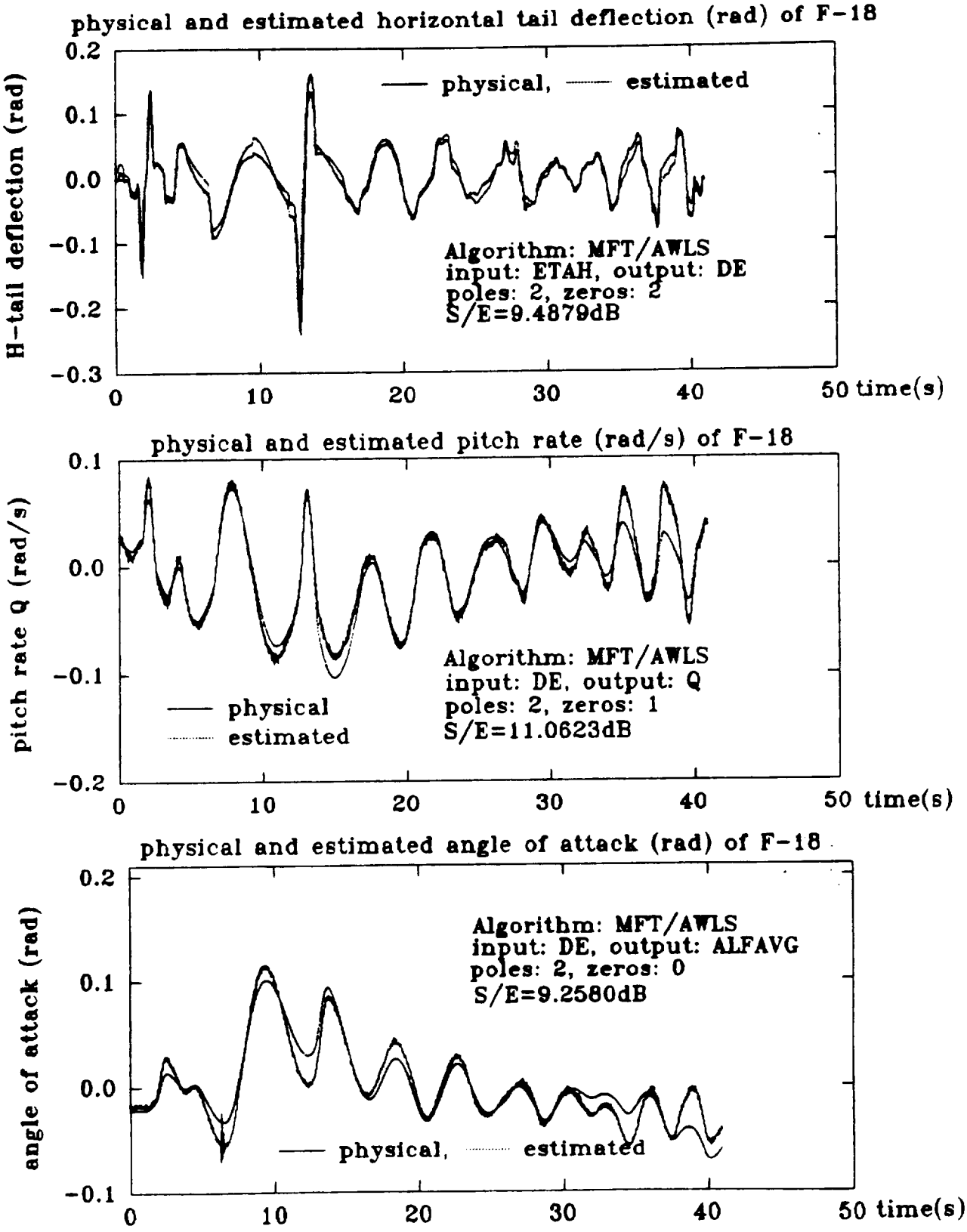

Fig. 8 Comparing the Physical and Model Responses

In addition to the visual comparison, a quantitative measure of how well the models perform is indicated on each graph as the "output signal-to-output error" ratio in decibels, which we define by

$$S/E = 20 \log_{10} \frac{\text{RMS}(y)}{\text{RMS}(e)}, \quad e(t) = y(t) - \hat{y}(t), \quad 0 \le t \le T \tag{20}$$

where RMS(y) means the root-mean-square value of the output signal $y(t)$ over the $[0,T]$ time interval, and $\hat{y}(t)$ is the estimated output using the model. Since our algorithm does not estimate initial conditions, we used a standard Luenberger observer running backwards in time (details omitted here) in order to determine an initial condition for each model output $\hat{y}(t)$ when comparing the signals depicted in Fig. 8.

A test to determine the sensitivity of the above models to shifts in the $[0,T]$ data sets is shown in Fig. 9 for a 200 point-shift. (The shifts in the pole-zero plots are smaller for shorter length point-shifts.) The scatter in the pole-zero plots reveal that the $H_{de}(s)$ model is the most sensitive of the three models in this regard.

As implied by the discussion in Section 3.2 above, we have been experimenting with two variations on the standard least squares algorithm using the Fourier based Modulating Function Technique (MFT). The symbols "LS", "WLS" and "AWLS" are used to distinguish respectively, the least squares estimates given by (15), (14) and (16)-(17). The models obtained using these three algorithms are compared in Figs. 10, 11 and 12 for the three subsystems. In addition to the visual comparison, the S/E ratios show that the adaptive weighted least squares algorithm is the best in each case.

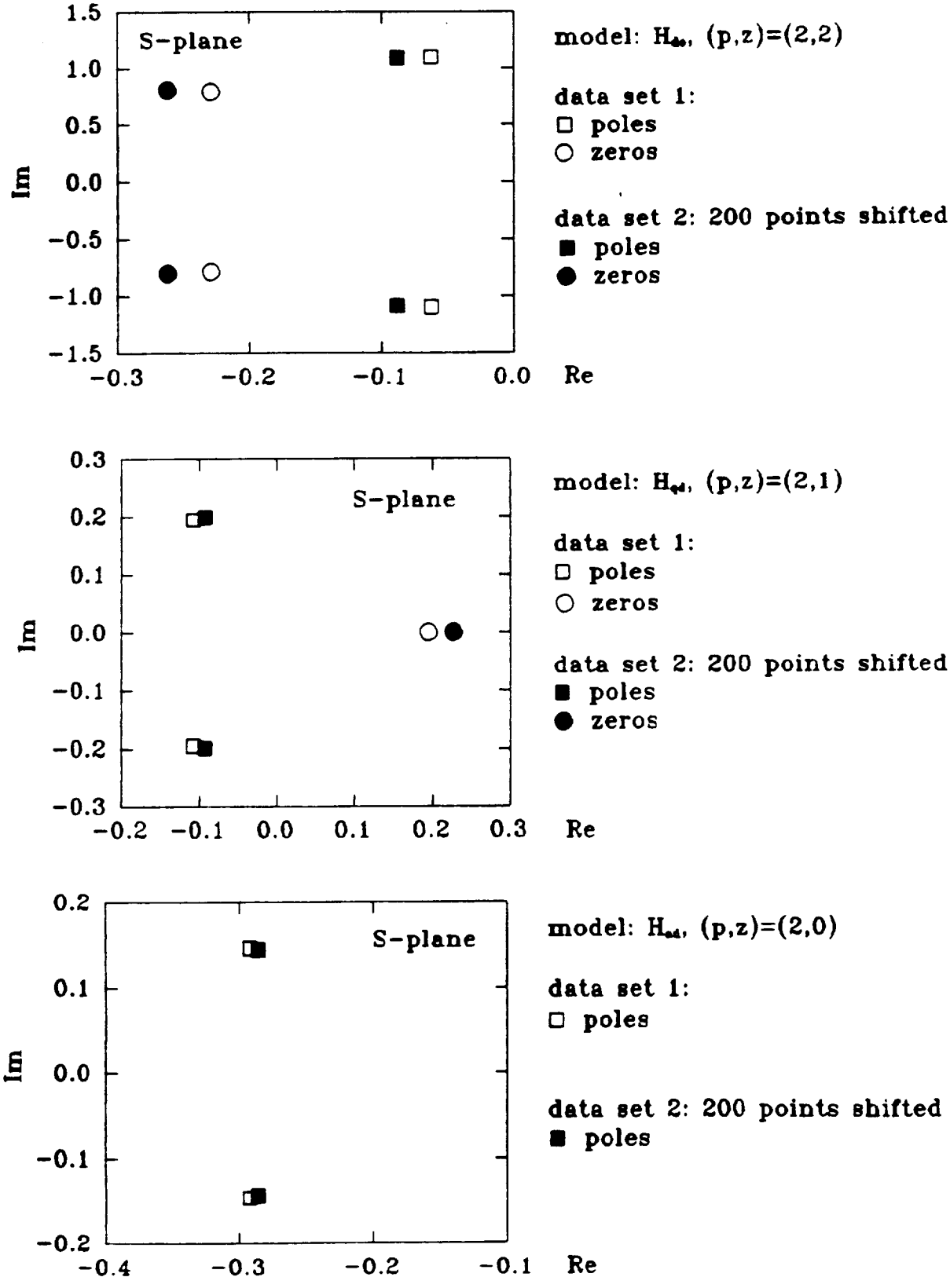

Fig. 9 Model Sensitivity to a Shifted Data Set

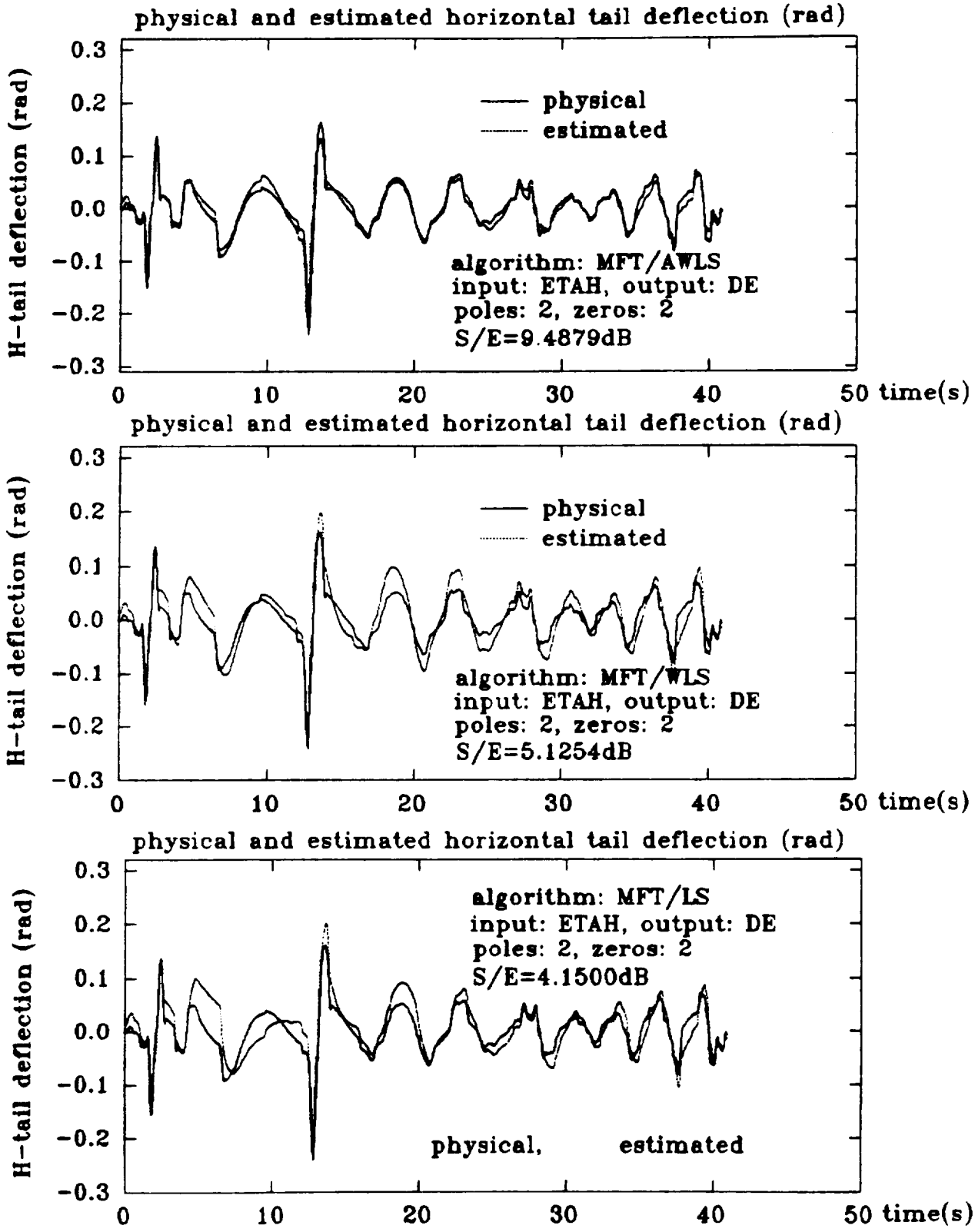

Fig. 10 Comparing $H_{de}(s)$ for AWLS, WLS and LS Algorithms

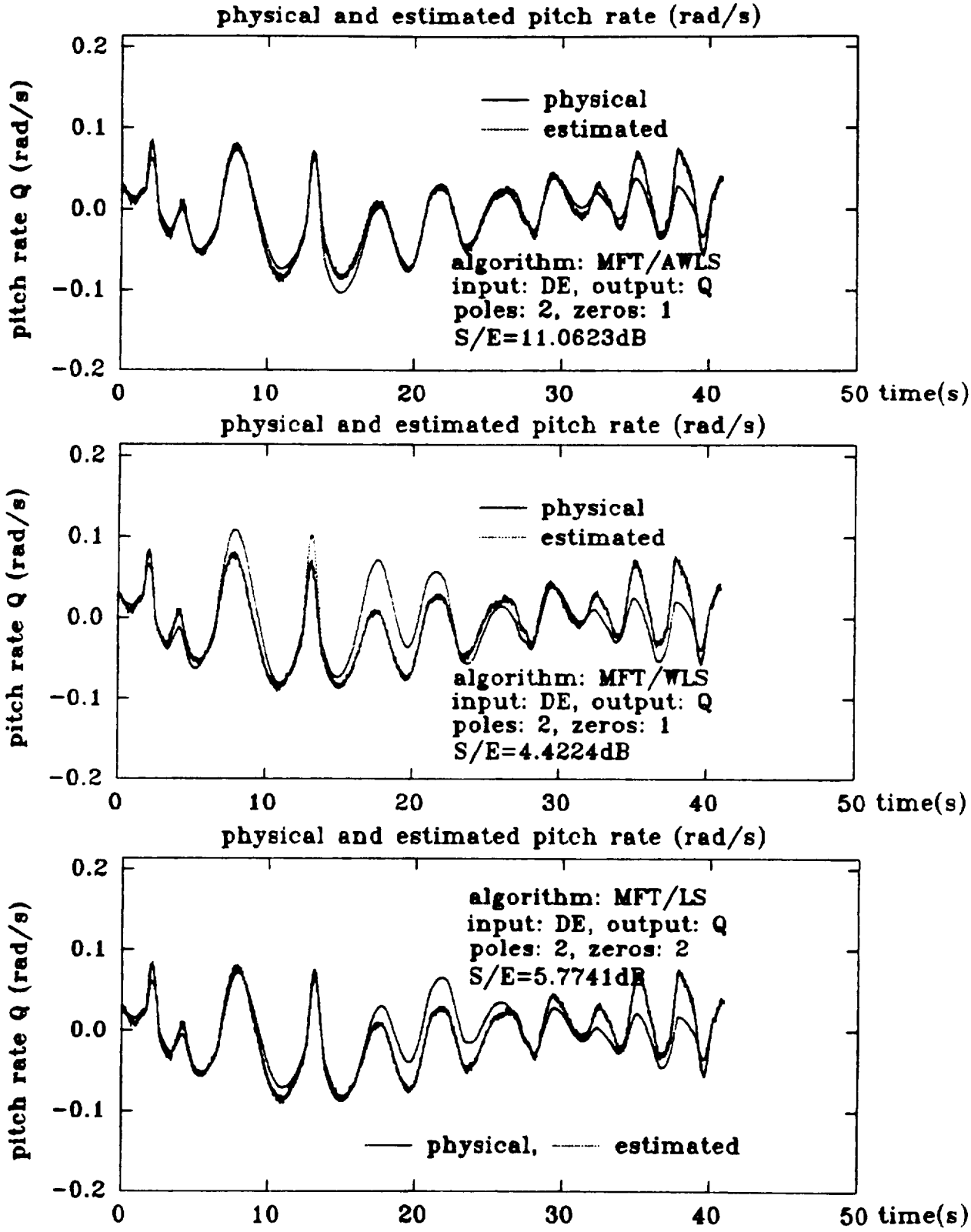

Fig. 11 Comparing $H_{qd}(s)$ for AWLS, WLS and LS Algorithms

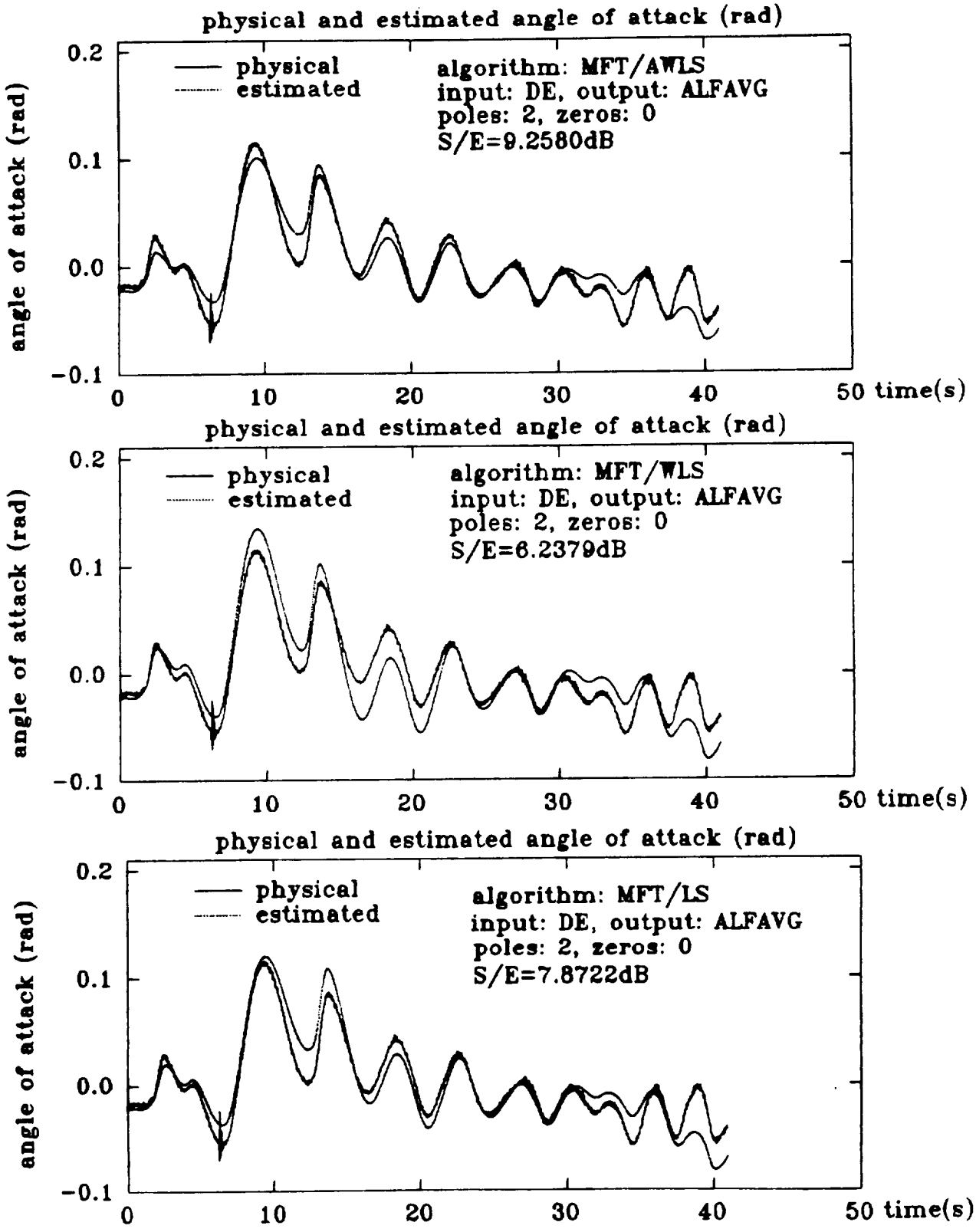

Fig. 12 Comparing $H_{ad}(s)$ for AWLS, WLS and LS Algorithms

Validation of the models with respect to the orders of the numerator and denominator polynomials in the transfer functions is the object of the materials presented in the remaining Figs. 13-22. The "AWLS" algorithm has been utilized for each of the models obtained in these figures. Quantitative data comparing various models for each subsystem is summarized in the "performance tables" of Figs. 13 and 14. As indicated in the tables, model orders up to and including 5 were tested. In addition to the S/E ratios, the minimum values of the criterion function J (defined in (10)) is shown in these tables for each pole/zero pair, as well as the stability property of the resulting model. Our best transfer functions summarized in Figs. 5-7 were based upon the data in these tables, though "best" is subject to some qualification. For example, using the notation "(2,0)" to imply a model with 2 poles and 0 zeros, and "(2,1)" a model with 2 poles and 1 zero, etc., the table for $H_{de}(s)$ in Fig. 13 shows that the (4,3), (4,4) and (5,4) models are each slightly better than the (2,2) model. However, the difference is not deemed significant enough to justify the more complex model and, therefore, the (2,2) model is offered as the best for $H_{de}(s)$. A further study of the residuals for the $H_{de}(s)$ substem is discussed below.

An inspection of Figs. 13 and 14 also reveals that unstable models were obtained for various structures, sometimes with quite respectable S/E ratios. Based upon the supposition that a stable model is preferred, a modification of the AWLS algorithm was tested that forced the model for the end result to be stable. [7] The performance tables for this "constrained" AWLS algorithm are shown in Figs. 15 and 16. This did not change the conclusion for the best models of $H_{de}(s)$ or $H_{qd}(s)$, but the conclusion for the $H_{ad}(s)$ is drawn into question by comparing the (2,0) and (4,2) models. The Bode and impulse response functions for these two models of $H_{ad}(s)$ are shown in Fig. 17 (also, the pole-zero plots). The differences are clearly minuscule. However, the predicted outputs for these two $H_{ad}(s)$ models is compared with the physical angle of attack output at the bottom of Fig. 16. Here it is seen that there is a noticeable improvement in the (4,2) model over the (2,0) model, but the advantage is probably not justified to warrant the additional complexity. Further comments regarding the residuals for the $H_{ad}(s)$ models are given below.

A study of the residuals for various models of the three subsystems is contained in Figs. 18-22. The two top graphs in each figure show respectively, the time and frequency plots of both the output signal and error signal $e=y-\hat{y}$. The bottom two graphs in each figure show the modulated residuals (on the LHS), and their normalized covariance (autocorrelation) as a function of the modulating frequency index (on the RHS). The χ^2 95% confidence limits for judging whether residuals are white, or not, are drawn in dotted lines in the lower right hand graph for each Fig. 18-22. Based upon this test, each of the models (more or less) can be accepted as the "true" model. Again, simplicity weighs towards the lower order model when two models satisfy this test as in the case of the $H_{de}(s)$ and $H_{ad}(s)$ subsystems.

---

[7] This was accomplished during the iterative solution of (16) and (17) by testing the stability of the system for each iterate of $\hat{\theta}_{awls}$, then starting the iterations over again (if unstable) using as a starting point the value of $\hat{\theta}_{awls}$ obtained by reflecting the unstable poles of the system about the imaginary axis thereby creating a stable system.

Performance table of model $H_{de}(s)$ under different structure assumptions

zeros / poles	0	1	2	3	4	5
1	s/e= -0.01dB **stable** $J=9.16\times10^{-9}$	s/e= -14.07dB unstable $J=3.41\times10^{-9}$				
2	s/e=0.42dB **stable** $J=6.87\times10^{-9}$	s/e=3.19dB **stable** $J=6.03\times10^{-9}$	s/e=9.49dB **stable** $J=7.22\times10^{-9}$			
3	s/e= -0.17dB unstable $J=6.21\times10^{-9}$	s/e= -107dB unstable $J=8.29\times10^{-10}$	s/e=3.55dB **stable** $J=2.59\times10^{-10}$	s/e= -3.66dB unstable $J=2.75\times10^{-11}$		
4	s/e=0.70dB **stable** $J=1.52\times10^{-7}$	s/e= -8.91dB unstable $J=1.23\times10^{-7}$	s/e=4.51dB **stable** $J=2.51\times10^{-7}$	s/e=10.28dB **stable** $J=1.16\times10^{-9}$	s/e=10.16dB **stable** $J=4.42\times10^{-10}$	
5	s/e=0.20dB unstable $J=1.25\times10^{-8}$	s/e= -96.97dB unstable $J=6.63\times10^{-9}$	s/e= -15.40dB unstable $J=2.87\times10^{-9}$	s/e=3.07dB unstable $J=3.59\times10^{-9}$	s/e=10.23dB **stable** $J=1.24\times10^{-11}$	s/e=4.03dB unstable $J=5.69\times10^{-12}$

s/e: signal-to-error ratio. J: criterion value. algorithm: unconstrained MFT/AWLS.

Performance table of model $H_{qd}(s)$ under different structure assumptions

zeros / poles	0	1	2	3	4	5
1	s/e= -2.28dB **stable** $J=3.39\times10^{-9}$	s/e= -2.28dB **stable** $J=3.22\times10^{-9}$				
2	s/e=1.02dB **stable** $J=1.02\times10^{-10}$	s/e=11.06dB **stable** $J=2.34\times10^{-11}$	s/e=11.24dB **stable** $J=2.60\times10^{-11}$			
3	s/e=1.82dB **stable** $J=4.92\times10^{-10}$	s/e=2.82dB **stable** $J=6.74\times10^{-10}$	s/e= -99.98dB unstable $J=4.04\times10^{-12}$	s/e= -93.76dB unstable $J=6.74\times10^{-12}$		
4	s/e=1.94dB **stable** $J=2.82\times10^{-10}$	s/e=0.69dB **stable** $J=1.99\times10^{-9}$	s/e= -25.70dB unstable $J=1.71\times10^{-9}$	s/e=1.24dB unstable $J=8.01\times10^{-13}$	s/e=0.62dB unstable $J=8.89\times10^{-13}$	
5	s/e= -5.36dB unstable $J=8.71\times10^{-10}$	s/e= -82.51dB unstable $J=8.17\times10^{-10}$	s/e= -74.19dB unstable $J=8.05\times10^{-10}$	s/e= -46.17dB unstable $J=1.18\times10^{-9}$	s/e= -18.51dB unstable $J=1.89\times10^{-11}$	s/e= -17.97dB unstable $J=1.93\times10^{-11}$

s/e: signal-to-error ratio. J: criterion value. algorithm: unconstrained MFT/AWLS.

Fig. 13 Performance Tables for Structure Determination of $H_{de}(s)$ and $H_{qd}(s)$

Performance table of model $H_{ad}(s)$ under different structure assumptions

zeros / poles	0	1	2	3	4	5
1	s/e=1.94dB **stable** J=2.39x10^{-9}	s/e=3.64dB **stable** J=1.41x10^{-9}				
2	s/e=9.25dB **stable** J=1.65x10^{-10}	s/e=9.17dB **stable** J=1.69x10^{-10}	s/e=4.54dB **stable** J=4.60x10^{-11}			
3	s/e=4.09dB **stable** J=1.22x10^{-9}	s/e=2.59dB unstable J=7.80x10^{-12}	s/e= -16.34dB unstable J=7.87x10^{-12}	s/e= -2.65dB unstable J=5.98x10^{-12}		
4	s/e= -123.7dB unstable J=2.68x10^{-11}	s/e= -112.0dB unstable J=3.61x10^{-11}	s/e=10.50dB unstable J=1.05x10^{-12}	s/e=9.90dB unstable J=1.01x10^{-12}	s/e=9.25dB **stable** J=7.17x10^{-13}	
5	s/e= -41.31dB unstable J=4.81x10^{-11}	s/e= -6.24dB **stable** J=8.01x10^{-13}	s/e= -5.06dB **stable** J=7.52x10^{-13}	s/e= -37.72dB unstable J=9.98x10^{-14}	s/e= -11.47dB unstable J=1.08x10^{-13}	s/e= -24.40dB unstable J=1.10x10^{-13}

s/e: signal-to-error ratio. J: criterion value. algorithm: unconstrained MFT/AWLS.

Fig. 14 Performance Table for Structure Determination of $H_{ad}(s)$

Performance table of model $H_{de}(s)$ under different structure assumptions

zeros / poles	0	1	2	3	4	5
1	s/e= -0.01dB stable J=9.10x10^{-9}	s/e=5.35dB stable J=3.65x10^{-9}				
2	s/e=0.42dB stable J=6.67x10^{-8}	s/e=3.19dB stable J=6.03x10^{-8}	s/e=9.49dB stable J=7.22x10^{-9}			
3	s/e= -0.09dB stable J=6.39x10^{-9}	s/e=0.79dB stable J=1.10x10^{-9}	s/e=3.55dB stable J=2.53x10^{-10}	s/e=8.99dB stable J=3.09x10^{-11}		
4	s/e=0.70dB stable J=1.52x10^{-7}	s/e=1.89dB stable J=1.51x10^{-7}	s/e=4.51dB stable J=2.51x10^{-7}	s/e=10.28dB stable J=1.15x10^{-9}	s/e=10.16dB stable J=4.42x10^{-10}	
5	s/e=0.27dB stable J=1.28x10^{-9}	s/e=0.98dB stable J=8.63x10^{-9}	s/e=1.77dB stable J=3.16x10^{-9}	s/e=4.19dB stable J=8.63x10^{-9}	s/e=10.23dB stable J=1.24x10^{-11}	s/e=9..71dB stable J=5.95x10^{-12}

s/e: signal-to-error ratio. J: criterion value. algorithm: constrained MFT/AWLS.

Performance table of model $H_{qd}(s)$ under different structure assumptions

zeros / poles	0	1	2	3	4	5
1	s/e= -2.28dB stable J=3.39x10^{-9}	s/e= -2.26dB stable J=3.23x10^{-9}				
2	s/e=1.02dB stable J=1.02x10^{-10}	s/e=11.06dB stable J=2.34x10^{-11}	s/e=11.24dB stable J=2.60x10^{-11}			
3	s/e=1.82dB stable J=4.92x10^{-10}	s/e=2.82dB stable J=6.74x10^{-10}	s/e= -1.88dB stable J=5.07x10^{-11}	s/e= -1.88dB stable J=8.99x10^{-11}		
4	s/e=1.94dB stable J=2.82x10^{-10}	s/e=0.63dB stable J=1.99x10^{-9}	s/e=2.31dB stable J=2.49x10^{-9}	s/e=4.92dB stable J=8.33x10^{-18}	s/e=4.86dB stable J=1.08x10^{-12}	
5	s/e=2.45dB stable J=9.12x10^{-10}	s/e= -4.55dB stable J=5.34x10^{-9}	s/e= -8.79dB stable J=4.08x10^{-9}	s/e= -2.44dB stable J=5.78x10^{-9}	s/e=2.58dB stable J=2.37x10^{-10}	s/e=3.01dB stable J=2.47x10^{-10}

s/e: signal-to-error ratio. J: criterion value. algorithm: constrained MFT/AWLS.

Fig. 15 Modified Performance Tables for the Constrained AWLS Algorithm

Performance table of model $H_{ad}(s)$ under different structure assumptions

zeros / poles	0	1	2	3	4	5
1	s/e=1.94dB **stable** J=2.89x10^{-9}	s/e=3.84dB **stable** J=1.41x10^{-9}				
2	s/e=9.25dB **stable** J=1.65x10^{-10}	s/e=9.17dB **stable** J=1.69x10^{-10}	s/e=4.54dB **stable** J=4.80x10^{-11}			
3	s/e=4.09dB **stable** J=1.22x10^{-9}	s/e=1.14dB **stable** J=2.81x10^{-11}	s/e= -0.85dB **stable** J=4.00x10^{-11}	s/e=1.29dB **stable** J=3.58x10^{-11}		
4	s/e= -1.00dB **stable** J=2.94x10^{-10}	s/e= -3.88dB **stable** J=3.19x10^{-10}	s/e=11.31dB **stable** J=1.16x10^{-12}	s/e=10.86dB **stable** J=1.20x10^{-12}	s/e=9.25dB **stable** J=7.17x10^{-13}	
5	s/e= -1.73dB **stable** J=2.05x10^{-10}	s/e= -6.24dB **stable** J=8.01x10^{-13}	s/e= -5.06dB **stable** J=7.52x10^{-13}	s/e=0.75dB **stable** J=7.72x10^{-13}	s/e= -0.56dB **stable** J=8.65x10^{-13}	s/e= -1.25dB **stable** J=2.99x10^{-13}

s/e: signal-to-error ratio. J: criterion value. algorithm: constrained MFT/AWLS.

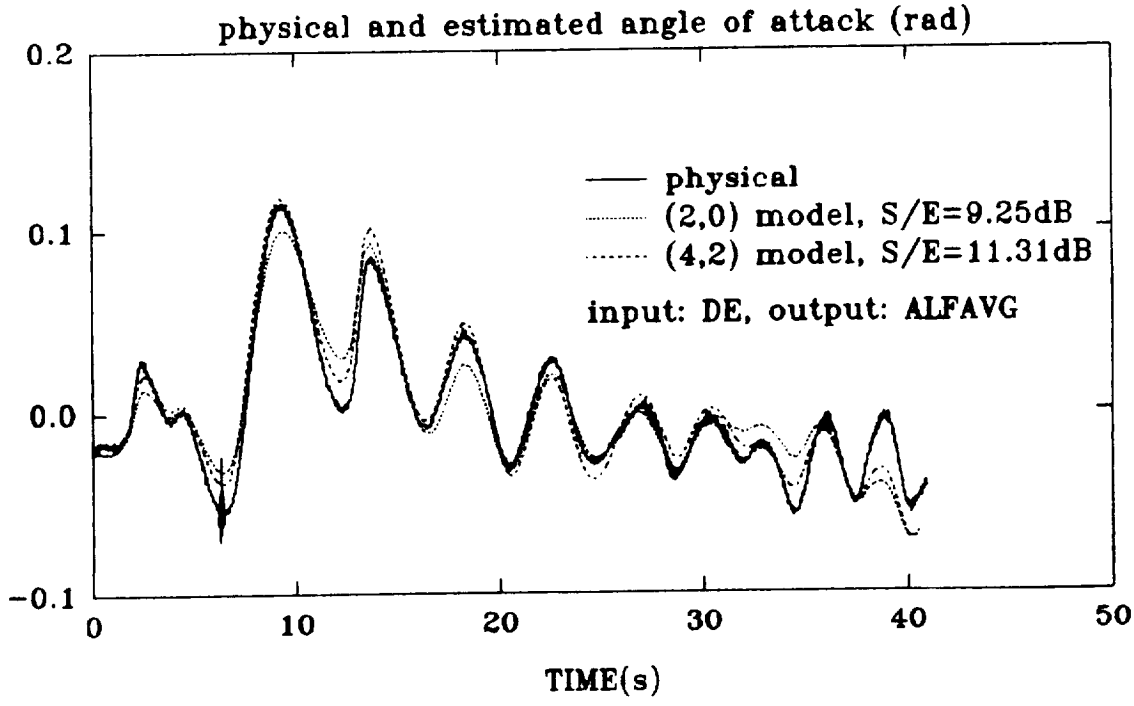

Fig. 16 Comparing $H_{ad}(s)$ Models for the Constrained AWLS Algorithm

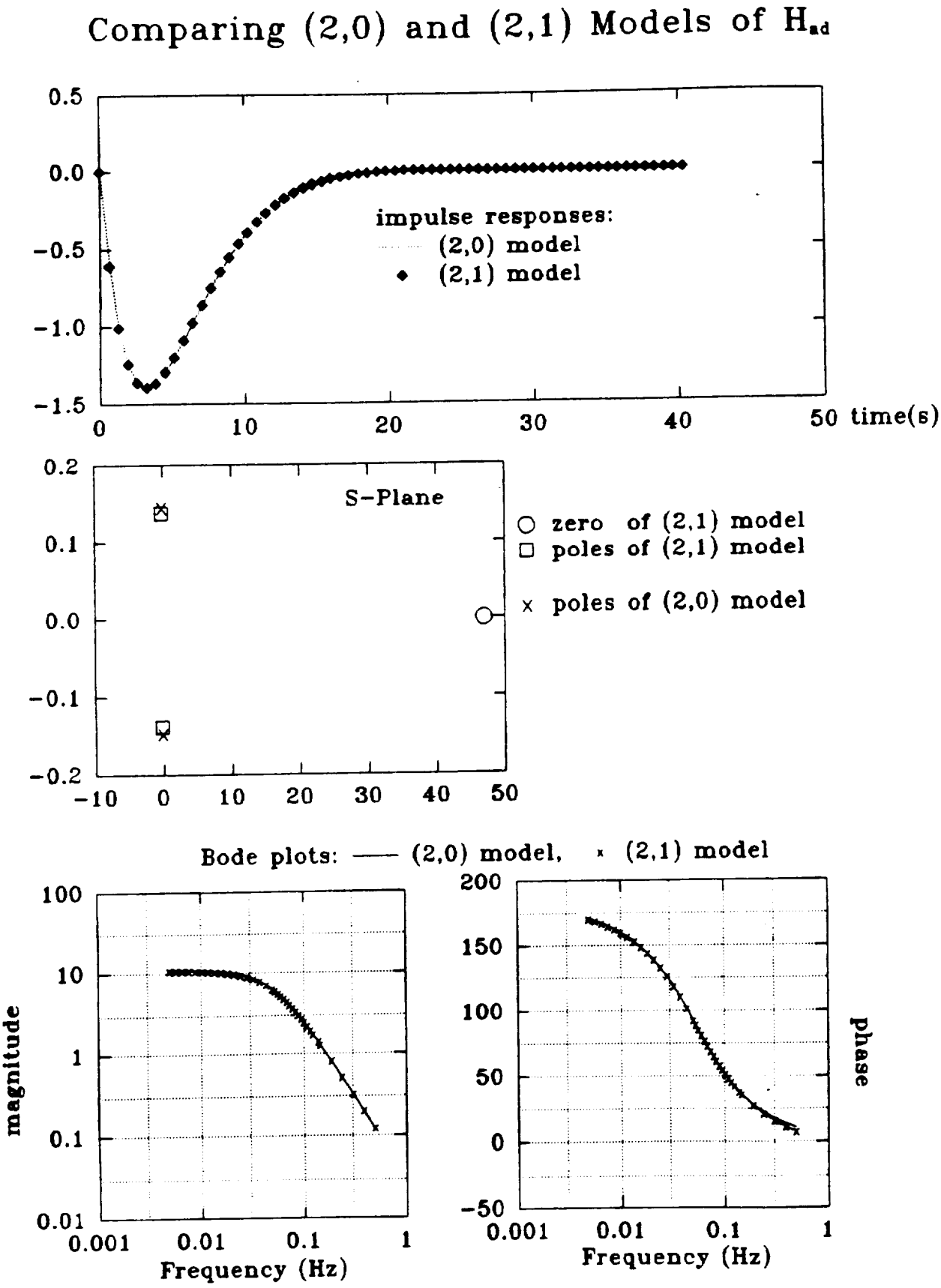

Fig. 17 Comparing Second Order $H_{ad}(s)$ Models

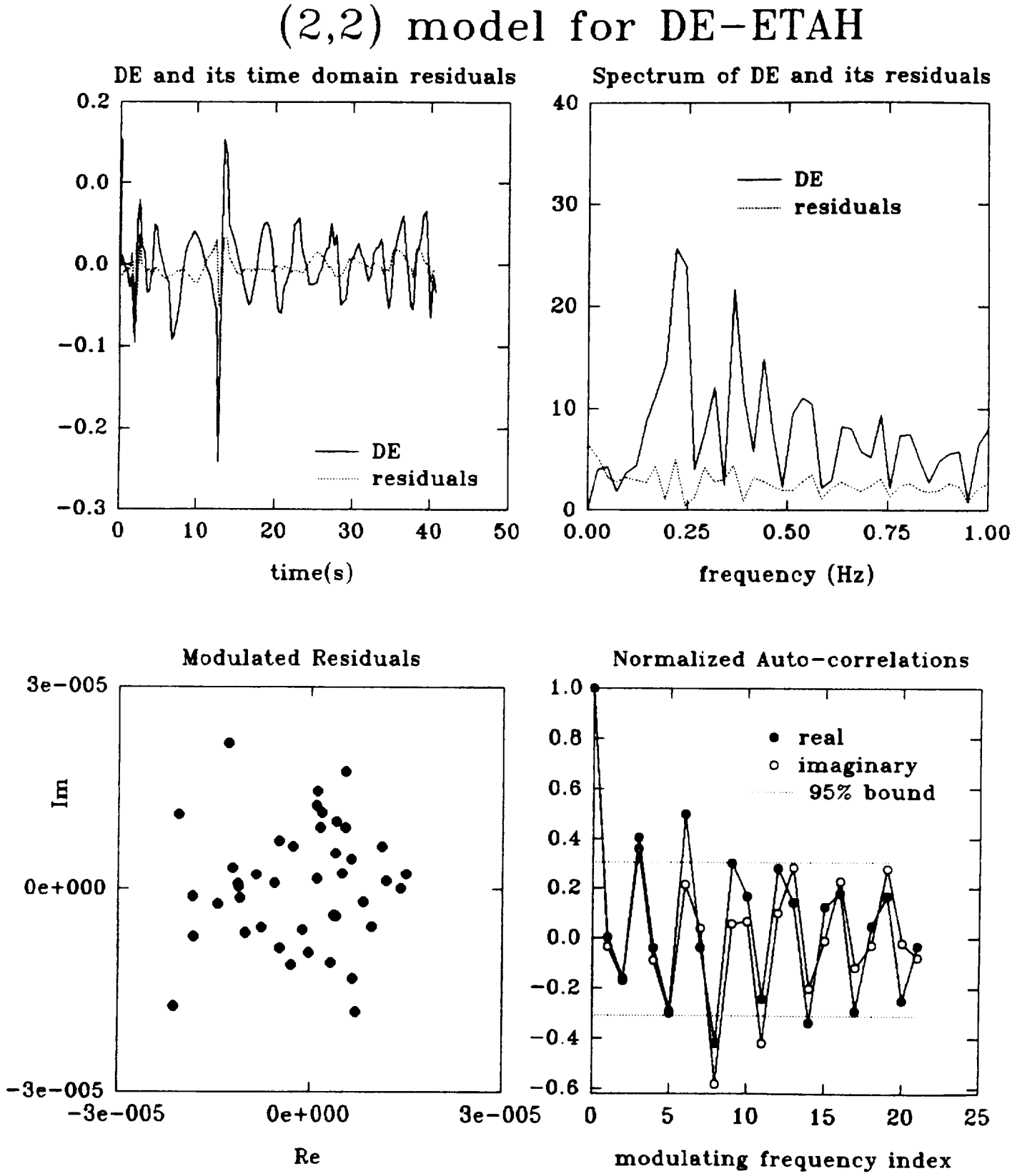

Fig. 18 Study of Residuals for the (2,2) $H_{de}(s)$ Model

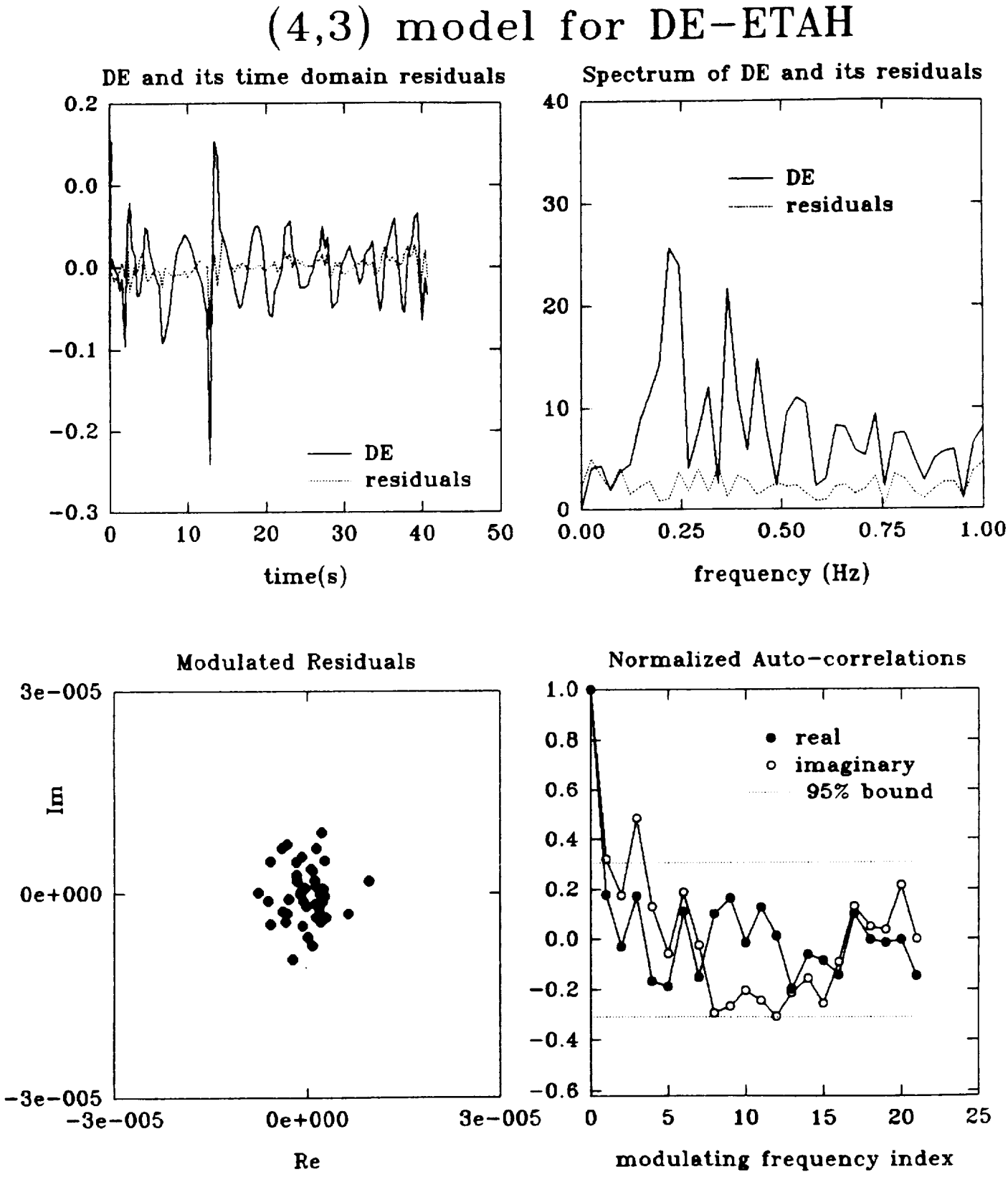

Fig. 19 Study of Residuals for the (4,3) $H_{de}(s)$ Model

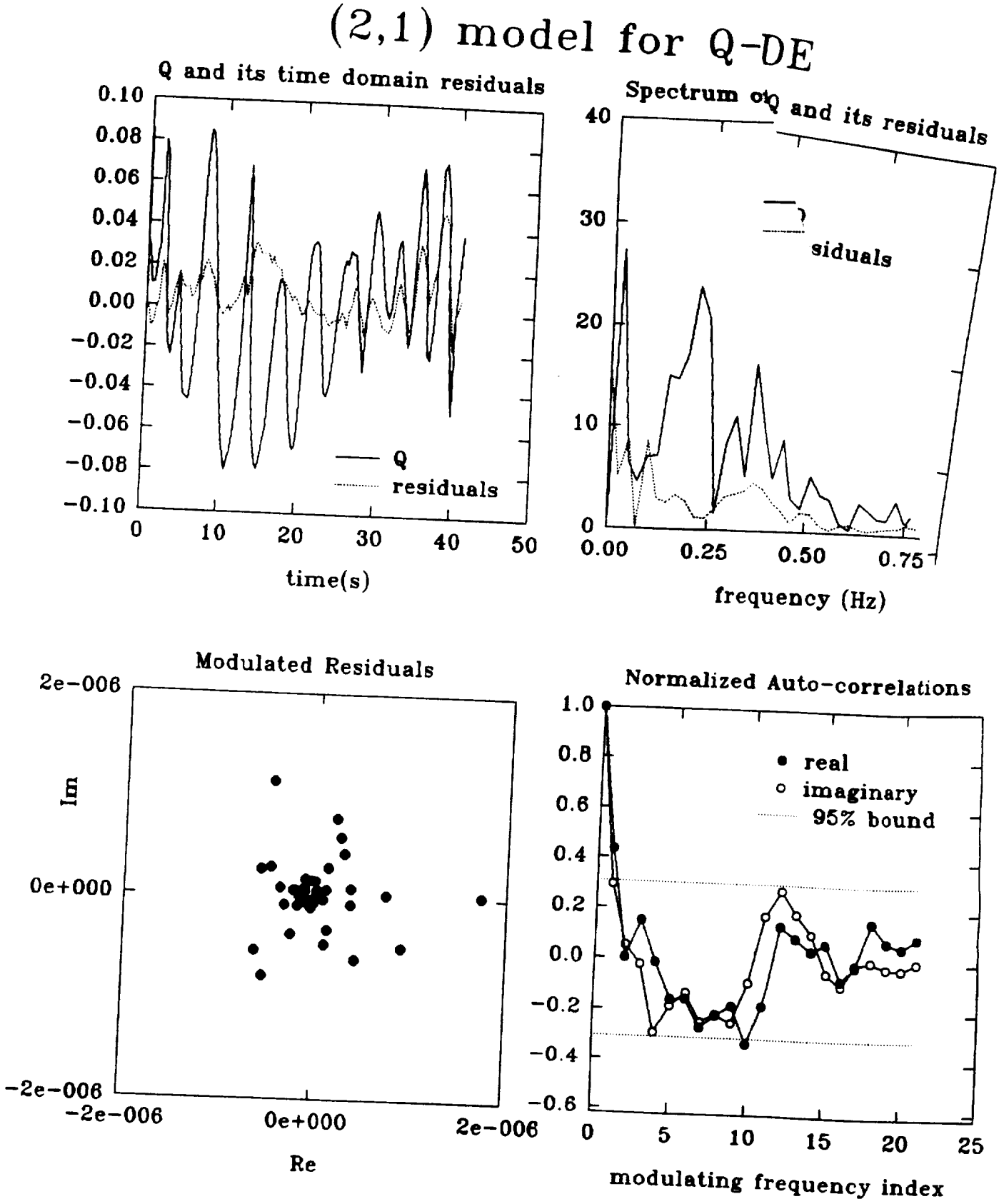

Fig. 20 Study of Residuals for the (2,1) $H_{qd}(s)$ Model

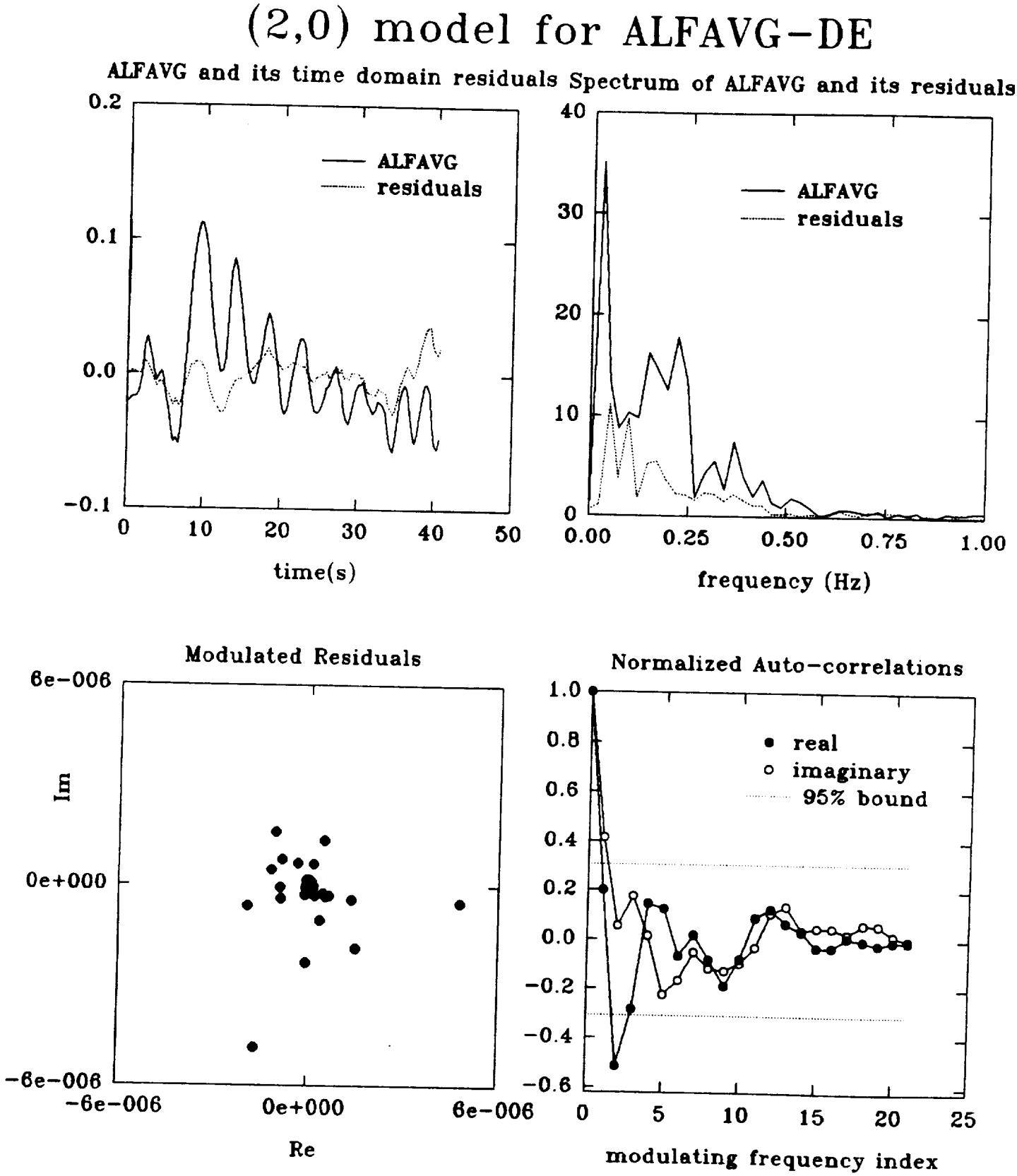

Fig. 21 Study of Residuals for the (2,0) $H_{ad}(s)$ Model

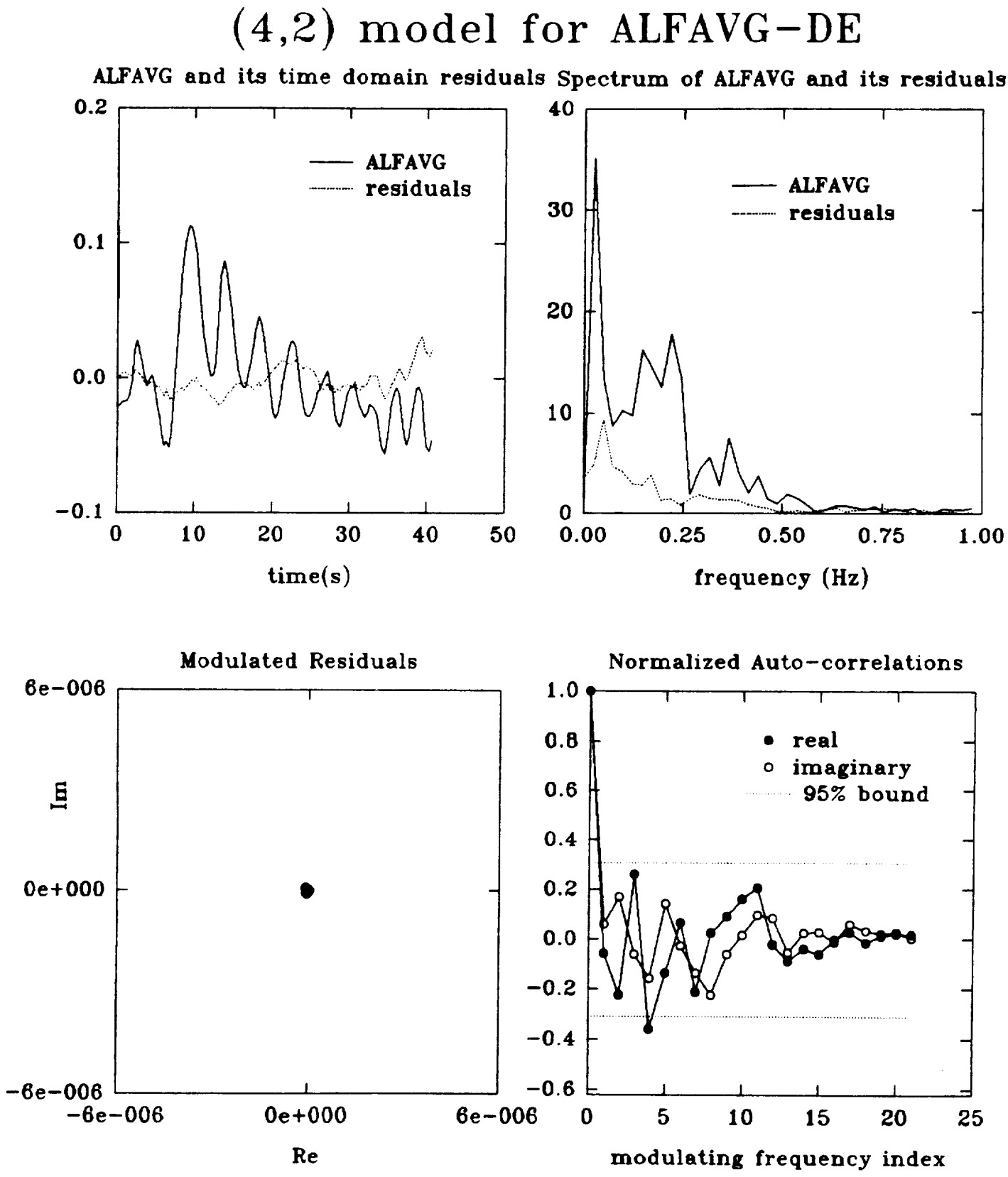

Fig. 22 Study of Residuals for the (4,2) $H_{ad}(s)$ Model

4. Future Research

We shall continue our investigations into modeling for the F-18 aircraft dynamics, focusing on the lateral dynamics as the next phase. We shall also consider obtaining the frequency transfer function models directly for this system using the theory put forth in [2], extended for MIMO systems. One further point of interest relates to the model reduction problem, which is the subject of Chapter 4 in Pan's thesis [1]. Shen has just rerun the two examples in Section 4.5 of [1] and found that the AWLS (adaptive weighted least squares) algorithm appears to give significantly better lower order approximations in the frequency domain than Pan's results which, in turn, were better than the methods in the literature with which Pan compared his algorithm. If this turns out to be generally true, then the weighted least squares formulation will have even broader utility than we anticipated.

5. Publications and Presentations

[1] Pan, J. Q., *System Identification, Model Reduction and Deconvolution Filtering Using Fourier Based Modulating Signals and High Order Statistics*. Ph. D. Dissertation, Brown University, Providence, RI, May 1992. Also, Technical Report LEMS-103, Division of Engineering, Brown University, March 1992.

[2] Pearson, A. E. and J. Q. Pan, "Frequency Analysis Via the Method of Moment Functionals." *Proceedings of the 30th IEEE CDC*, Brighton, UK, Dec. 1991.

[3] Pan, J. Q. and A. E. Pearson, "High Resolution Frequency Estimation in the Presence of Noise Using Complex Sinusoidal Modulating Signals." Presented at *The 26th Conf. on Inform. Sci. and Systems*, Princeton Univ., Princeton, NJ, March 1992.